Formation and stability of band patterns in a rotating suspension-filled cylinder

G. Seiden,[1,*] M. Ungarish,[2] and S. G. Lipson[1]
[1]*Department of Physics, Technion-Israel Institute of Technology, Haifa 32000, Israel*
[2]*Department of Computer Science, Technion-Israel Institute of Technology, Haifa 32000, Israel*
(Received 9 March 2007; published 31 August 2007)

We explore the phenomenon of segregation and pattern formation in the complex system of a rotating horizontal cylinder completely filled with a dilute suspension of non-Brownian particles. A general dimensionless analysis is presented, which reveals the importance of the different dimensionless parameters involved. A detailed account of the mechanism of segregation and formation of axial bands for the case of low viscosity fluids is given. According to the analysis the axial pressure gradient associated with an inertial-mode excitation within the bounded fluid is responsible for the formation of bands in interleaving nodal planes of the excitation. The question of stability of the band patterns is addressed and a phase diagram in the appropriate dimensionless space is presented.

DOI: 10.1103/PhysRevE.76.026221 PACS number(s): 89.75.Kd, 82.70.−y, 45.70.Qj, 47.54.−r

I. INTRODUCTION

The different self-organizing systems related to the configuration of a rotating horizontal cylinder can be divided into three groups. The first group is that of mixtures of granular materials, which when placed in the rotating cylinder exhibit both radial and axial patterns and which has been extensively investigated (see [1] and the references therein). To the second group belong systems consisting of a suspension which partially fills a rotating horizontal drum [2–5]. The third, which we explore here, consists of suspensions which completely fill the rotating cylinder [6–12]. Though the observed patterns in the three groups seem quite similar, the physical origin is very different. Moreover, even within a particular group the mechanism of segregation and formation of bands can be quite different [3,4].

In general, the spontaneous segregation into axial band patterns of a suspension which completely fills a rotating horizontal cylinder can be described in the following way. An initially homogenous distribution of negatively buoyant suspended particles[1] induces a downward force on the embedding fluid, which in turn tends to cause a net flow in the direction of gravity. Conservation of the continuous phase then results in convectionlike cells being formed, which carry the particles to optimal planes where they continue to enforce a stable time independent flow pattern.

Several experimental investigations of the banding phenomenon in a suspension which completely fills a rotating horizontal cylinder have been carried out in recent years, which have revealed its main features. Lipson [6] and Lipson and Seiden [7] observed the phenomenon for NH_4Cl crystals suspended in their supersaturated solution and for different millimeter-sized particles (e.g., 3 mm polystyrene balls) suspended in water. Breu *et al.* [8] reported the phenomenon for 300 μm glass balls suspended in water. The different stages were studied while varying the rotation frequency. When bands were observed two periodic lengths of either $\Lambda=3.56R$ or $\Lambda=2.68R$ (R being the tube radius) were measured, though the dominant spacing was the former. Matson *et al.* [9] have investigated the banding phenomenon for somewhat more viscous suspensions (10 cP–70 cP), which contained 100 μm glass balls. They, too, have investigated the different scenarios observed as the rotation rate varied. A phase diagram of the different states was drawn and a detailed account of the interfaces between the different phases was given. The periodic spacing in these experiments was $\Lambda=2.4R$. Seiden *et al.* [11,12] have carried out a series of experiments in which they investigated the dependence of the periodic length on the tube length as well as the dependence of the phenomenon on particle characteristics (i.e., dimension, shape, and specific gravity) and fluid viscosity. The dominant periodic length in their experiments was $\Lambda\cong 3.6R$, though a tendency towards $\Lambda=4R$ was observed for long tube lengths. In all of the above experiments the volume fraction was close to 1%, which implies a dilute suspension.

Unlike the case of banding of suspended particles in a partially filled rotating horizontal cylinder where the reported values of viscosity are relatively high [$O(10\ \mathrm{P})$], in the case of suspensions which completely fill a rotating cylinder the values associated with the phenomenon are in general smaller than 1 P. This led Seiden *et al.* [12] to theoretically investigate the low viscosity limit using a boundary layer approach. Their conclusion was that, viewed from a rotating frame of reference, the suspended particles continuously excite inertial modes which in turn cause segregation into well-defined bands, coinciding with interleaving nodal planes of the wave excitation.

In this work we further investigate the mechanism of segregation and formation of axial bands in the suspension-filled rotating horizontal cylinder. In Sec. II we present a general dimensionless analysis aimed at revealing the different dimensionless parameters associated with the phenomenon and their relevance to the occurrence of the band patterns. Section III analyses the motion of a single suspended particle through the rotating fluid core. Then, in Sec. IV, we focus our

*Present address: Max Planck Institute for Dynamics and Self-Organization, Goettingen 37073, Germany. gabriel.seiden@ds.mpg.de

[1]The situation is practically symmetric for positively buoyant particles.

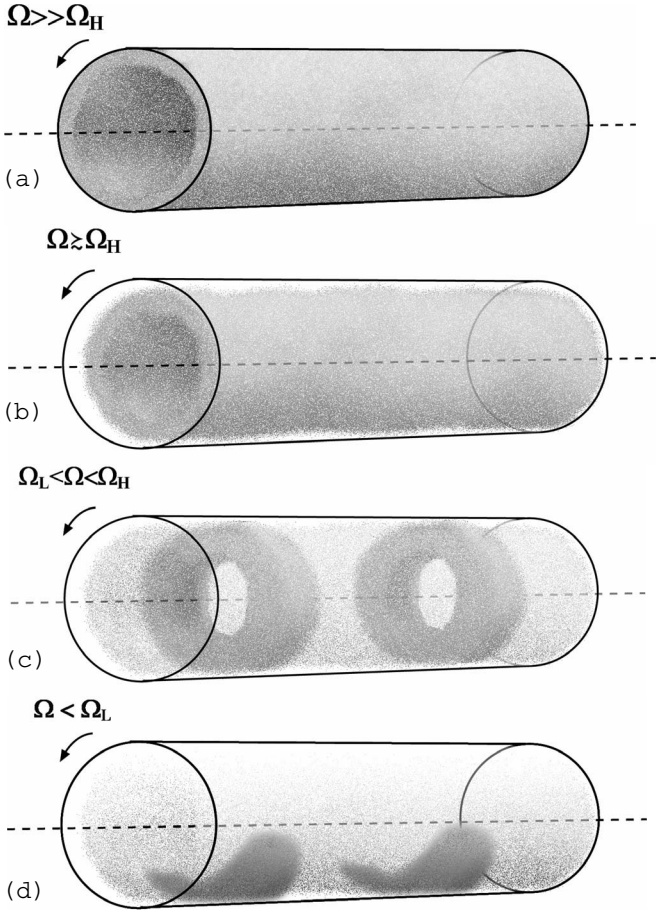

FIG. 1. Graphically designed illustration of different stages observed for a suspension of heavy particles completely filling a rotating horizontal cylinder. (a) For very high frequencies the suspension forms a thin coating on the inner cylinder surface. (b) Just above the critical frequency (Ω_H) the suspended particles form an off-centered tube. (c) In the interval $\Omega_L<\Omega<\Omega_H$ stable, periodically spaced, bands are observed. (d) Lowering the rotation frequency below Ω_L results in the breakdown of the suspended bands.

attention on the low viscosity regime and describe in detail the axial forces which cause segregation into well-defined periodically spaced bands. The question of the stability of the band patterns is also addressed in this section.

II. GENERAL DIMENSIONLESS CONSIDERATION

Figure 1 presents a graphical illustration of the main stages observed when the rotation frequency, Ω, of the bounding cylinder is varied, all other parameters kept unchanged. The two indicated frequencies, Ω_H and Ω_L, are critical frequencies marking the stability range of the bands. If the rotation frequency is much higher than Ω_H [Fig. 1(a)], the suspension forms a thin coating adjacent to the cylinder surface due to the centrifugal effect. When the frequency is lowered towards the upper critical frequency, the particles detach from the wall and form an off-centered tube [Fig. 1(b)]. Then, when Ω_H is reached, segregation takes place into one of two possible (degenerate) stable, periodically spaced, band patterns [Fig. 1(c)]. This state is stable until, when reaching Ω_L, the bands contract and collapses [Fig. 1(d)]. In some instances (e.g., for 3 mm polystyrene balls suspended in water [11]), oscillations between the two degenerate patterns precede the breakdown of the suspended, ring shaped, bands.

An important question from a theoretical point of view concerns the dimensionless parameters, each of which conveys a physical principle underlying the origin of the banding phenomenon. When specified, these parameters would indicate whether for a given arbitrary system segregation into bands would occur and more generally allow for the identification of the stability region in the corresponding parameter space. In general a given system is defined by nine[2] physical dimensional parameters. These are the particle dimension[3] (d) and density (ρ_p), the fluid dynamic viscosity (η) and density (ρ_f), the cylinder radius (R), length (L), and constant rotation frequency (Ω), the gravity-buoyancy force $[(\rho_p-\rho_f)g]$, and the volume of the dispersed phase (V_p). These include three dimensions and therefore, according to Buckingham's Π theorem [13], there should be six dimensionless numbers associated with the phenomenon. The temperature dependence of the thermodynamic parameters is assumed negligible in our discussion.

In what follows we present the dimensionless parameters from a physically insightful point of view. A more rigorous derivation of these parameters is given in the Appendix. Out of the six dimensionless parameters, four are principal with regard to the question of the occurrence of the banding phenomenon. The first three concern the motion of a single particle in the otherwise rigidly rotating fluid. In this respect an important point to note is that segregation only occurs if the particles detach from the cylindrical surface and penetrate the rigidly rotating core. This obviously requires the particles to be non-neutrally buoyant (positively or negatively). The first parameter is given by the ratio of centrifugal to gravity-buoyancy forces:

$$\Pi_1 = \rho_p \Omega^2 R/\Delta\rho g,$$

where $\Delta\rho=\rho_p-\rho_f$. The second is the ratio of the centripetal force, resulting from the pressure gradient in the fluid, and the buoyancy force,

$$\Pi_2 = \rho_f \Omega^2 R/\Delta\rho g.$$

These parameters, and in particular Π_1, indicate whether or not the particle will detach from the wall. Examining the question of detachment at the uppermost point on the cir-

[2]We exclude collision (particle-wall and particle-particle) parameters such as coefficients of restitution and surface roughness, which are believed to have negligible effect on the banding mechanism at the *dilute suspension limit*. We refer to the effect of collisions in more detail when presenting numerical simulations of particle trajectories (see Sec. III).

[3]In what follows we primarily deal with the case of spherical particles. The main results of the paper are nevertheless expected to hold for particles of different shapes as the features of the banding phenomenon were shown to be independent of this aspect [12].

cumference of the cylinder, we have the approximate detachment criterion,

$$\frac{\rho_p \Omega^2 R}{\Delta\rho g + \rho_f \Omega^2 R} = \frac{\Pi_1}{(1+\Pi_2)} < 1.$$

For values of Π_1 much greater than unity the particle will be pinned to the tube's surface, while for values much smaller than unity the particle will remain at the bottom of the tube. Typical empirical values for Π_1 and Π_2 range between $O(0.01)$ and $O(1)$.

The third parameter describes the balance between the drag force and gravity-buoyancy force,[4]

$$\Pi_3 = 18\eta\Omega R/\Delta\rho g d^2.$$

Optimal values for this ratio ensure that the particle, once landing on the bottom of the cylinder, will be dragged back by the viscous force to its detachment point. Typical empirical values for Π_3 are $O(1)$ though cases corresponding to higher values have been reported for small particles [9]. The fourth dimensionless parameter is the volume fraction

$$\Pi_4 = V_p/\pi R^2 L.$$

For very small values of Π_4 (i.e., $\Pi_4 \ll 1\%$) the phenomenon does not occur and the particles are not attracted to specific periodic planes. In all the cases studied experimentally the value of Π_4 was close to 1%.[5]

Other dimensionless parameters, which are of secondary importance in determining whether segregation will take place, are the Reynolds number based on the particle dimension and wall velocity, $\Pi_5 = \mathrm{Re}_d = \rho_f d\Omega R/\eta$, and the Reynolds number based on the tube radius and wall velocity, $\mathrm{Re}_R = (\Pi_3/18\Pi_2)\Pi_5^2 = \rho_f \Omega R^2/\eta$. The former, combined with the first three dimensionless parameters, determine the actual stationary trajectory of the particle through the rigidly rotating fluid [see Eq. (2) below], while the latter determines whether or not boundary effects are important (in what follows we will be referring to its reciprocal—the Ekman number). The Stokes number, $\mathrm{St} = \Pi_5\Pi_1/9\Pi_2 = \rho_p \Omega R d/9\eta$, is important in determining the relevant values of the restitution coefficients for particle-wall collisions. The sixth independent dimensionless parameter is the aspect ratio: $\Pi_6 = L/R$. It is worth noting that in the low-viscosity regime a preference for discrete values of Π_6 (i.e., $L/R \cong 2n$ where n is an integer) is observed. Moreover, the intriguing phenomenon of oscillating bands is strongly related to those values [12].

III. EQUATION OF MOTION FOR SINGLE PARTICLE

Understanding the motion of a single particle through the fluid core seems to be of importance in revealing the physical origin of the spontaneous formation of bands, especially in the dilute suspension limit [8,10,12]. We now attempt to approximate the drag force acting on a suspended particle while in motion through the otherwise rigidly rotating fluid. This will enable us to write down a closed form for the equation of motion, which we will then solve numerically and compare with a relevant experimental result. In determining the drag acting on the solid particle, distinction should be made between the motion through the fluid core (away from the wall) and motion adjacent to the wall. In the latter the particle undergoes a complex slip-roll motion and the drag is generally greater due to the presence of the wall.

Previous theoretical investigations of the motion of a nonneutrally buoyant particle suspended in a rotating horizontal cylinder dealt with the Stokes limit (i.e., $\mathrm{Re}_d \ll 1$). Roberts *et al.* [14] have solved the linear governing equation analytically, with the intention of finding bounds on the rotation rate which will insure that the trajectory of the particle is confined to the interior of the cylinder. Breu *et al.* [8] have numerically calculated the trajectory of a suspended particle through the fluid core from its detachment point to its landing point. They have taken into consideration the effect of the wall as the particle approaches its vicinity, but have not considered the motion of the particle when adjacent to the wall. The treatment below is an extension of these works to the case of nonvanishing Reynolds numbers.

We ascribe an empirical law for the drag acting on the particle [15] which assumes a steady motion through an otherwise quiescent infinite fluid, with velocity equal to the instantaneous relative velocity of the particle with respect to the fluid. This is the prime component of the drag in more elaborate considerations of the unsteady motion of a particle through a fluid in the non-negligible Reynolds number regime [16]. The equation of motion for the suspended particle is

$$m_p \ddot{\mathbf{r}} = -3\pi\eta d\{1 + f[\mathrm{Re}(|\dot{\mathbf{r}} - \mathbf{u}|)]\}(\dot{\mathbf{r}} - \mathbf{u}) - \frac{m_f}{\rho_f}\nabla\tilde{p} + m_b \mathbf{g}. \tag{1}$$

In the above $\mathbf{u}$ is the given fluid velocity, $\tilde{p} = p + \rho_f(\Omega \times \mathbf{r})^2$, where p is the dynamical pressure, $m_{p,f} = \frac{\pi}{6}\rho_{p,f} d^3$, $m_b = \frac{\pi}{6}\Delta\rho d^3$, $\mathrm{Re}(|\dot{\mathbf{r}} - \mathbf{u}|) = \frac{\rho_f d|\dot{\mathbf{r}} - \mathbf{u}|}{\eta}$, and f is given by the relevant (Reynolds number dependent) empirical drag law.

Next we seek the dimensionless form of Eq. (1). To this end we use the scaled variables:

$$t^* = \Omega t, \quad \mathbf{r}^* = \mathbf{r}/R, \quad \mathbf{u}^* = \mathbf{u}/\Omega R, \quad \tilde{p}^* = \tilde{p}/\rho_f \Omega^2 R^2.$$

Substituting into Eq. (1) and dividing both sides by $m_b g$ yields

$$\Pi_1 \ddot{\mathbf{r}}^* = -\Pi_3\{1 + f[\mathrm{Re}(|\dot{\mathbf{r}}^* - \mathbf{u}^*|)]\}(\dot{\mathbf{r}}^* - \mathbf{u}^*) - \Pi_2 \nabla^* \tilde{p}^* + \hat{\mathbf{q}}, \tag{2}$$

where $\mathrm{Re}(|\dot{\mathbf{r}}^* - \mathbf{u}^*|) = \Pi_5|\dot{\mathbf{r}}^* - \mathbf{u}^*|$ and $\hat{\mathbf{q}}$ is a unit vector in the direction of gravity. Thus, given the dimensionless coefficients Π_1, Π_2, Π_3, and Π_5, the trajectory of the particle through the fluid core is determined.

[4]Here we assume a Stokes drag. A better assessment of Π_3 requires knowledge of the Reynolds number (Π_5). For relatively large Π_5, an appropriate empirical law can be used (cf. Ref. [15]).

[5]We will elaborate on the physical significance of Π_4, as well as of Π_6, in the discussion section.

As mentioned earlier, the motion in the close vicinity of the cylindrical wall is quite different and now we have to make further assumptions regarding the collision with the wall and the drag acting on the particle while adjacent to the cylindrical surface. Considering the collision with the cylindrical surface, we note that the relevant Stokes number (St), which is the main dimensionless parameter determining whether the particle will bounce off the wall [17,18], is generally less than the marginal value above which rebound is observed (St $\sim$ 10) and thus we conclude that the sphere does not bounce off the wall. The tangential velocity is assumed to be unchanged during the collision.

For the complex motion in the segment adjacent to the wall we define a numerical wall-drag parameter, β_1, which multiplies the empirical drag in Eq. (2). Another numerical parameter used, β_2, concerns the width of the boundary layer at the curved cylindrical surface. It indicates the measure to which the tangential velocity components of a perturbation field decays in the vicinity of the wall. This last parameter will be relevant when examining the validity of the theoretical perturbation field with regard to inducing axial migration of the suspended particles and the ultimate formation of bands (see Sec. IV). The width of the curved boundary layer in most of the experiments reported is estimated to be of the order of 1 mm.

We test the numerical scheme, an explicit Euler simulation, first for the low Reynolds number scenario and compare with the analytical solution of Roberts *et al.* [14]. Figure 2(a) shows the numerical (solid line) and analytical (circles) trajectories of a 50 μm ball suspended in a fluid-filled horizontal cylinder having an inner diameter of 50 mm and rotating at $\Omega=0.4$ rad/s. The ball's density is 1.5 g/cm^3 and the fluid density and viscosity are 1 g/cm^3 and 1 cP, respectively. The ball is initially at rest at $(r,\phi)=(18.75,\pi)$. A very good agreement with the theoretical prediction is observed.

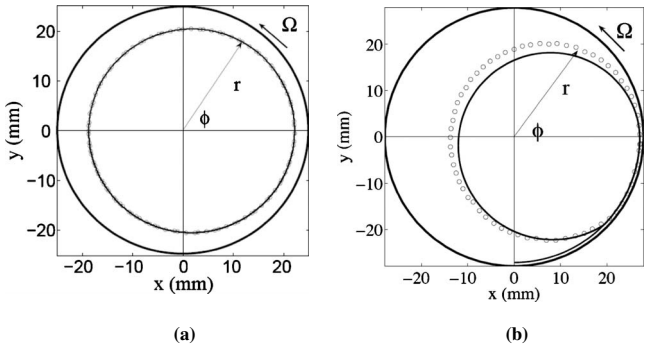

FIG. 2. (a) Numerical (solid line) and theoretical (circles) trajectories for the low Reynolds number regime ($\Pi_5=0.05$). (b) Numerical (solid line) and experimental (circles) results for the projection of the trajectory of a 1.59 mm Nylon ball in a water-filled rotating horizontal cylinder. The inner tube diameter is 55.8 mm and the rotation rate is 4.9 rad/s.

Next, we test the numerical code for the case of a suspended sphere in a rigidly rotating flow (no inertial mode), and compare the trajectory projection onto the $r-\phi$ plane with the experimental study of the same scenario. Figure 2(b) shows the results of a simulation, done for a 1.59 mm Nylon ball suspended in a water-filled cylinder having an inner diameter of 55.8 mm. The correction to the Stokes drag used in the simulation corresponds to the relevant instantaneous Reynolds number [$\mathrm{Re}(|\dot{\mathbf{r}}^*-\mathbf{u}^*|)$] ranges [15],

$$f[\mathrm{Re}(|\dot{\mathbf{r}}^*-\mathbf{u}^*|)]=\begin{cases}0, & 0<\mathrm{Re}(|\dot{\mathbf{r}}^*-\mathbf{u}^*|)<0.01,\\ 0.1315\,\mathrm{Re}(|\dot{\mathbf{r}}^*-\mathbf{u}^*|)^{[0.82-0.05\log_{10}\mathrm{Re}(|\dot{\mathbf{r}}^*-\mathbf{u}^*|)]}, & 0.01<\mathrm{Re}(|\dot{\mathbf{r}}^*-\mathbf{u}^*|)<20,\\ 0.1935\,\mathrm{Re}(|\dot{\mathbf{r}}^*-\mathbf{u}^*|)^{0.6305}, & 20<\mathrm{Re}(|\dot{\mathbf{r}}^*-\mathbf{u}^*|)<260.\end{cases} \tag{3}$$

The value of the numerical wall-drag parameter was varied in the range $1\leqslant\beta_1\leqslant 3$ with no significant effect observed on the particle trajectory. The particle is initially at rest at the bottom of the cylinder. It then acquires a stationary trajectory in the $r-\phi$ plane. The figure shows a good agreement between the numerical result and the experimental realization. This is of particular importance as the Reynolds number in this instance is relatively high, $\mathrm{Re}_d\approx 200$.

IV. THE LOW VISCOSITY REGIME

A. Mechanism of segregation and formation of bands

A theoretical explanation of the banding phenomenon was given by Seiden *et al.* [12], whereby the segregation into periodic axial bands results from a mutual interaction between the suspended particles and inertial modes excited in the bounding cylinder. Inertial modes are solutions of the linearized Navier-Stokes equations in a rotating frame of reference [19]. The theory assumes small perturbations to the rigidly rotating flow and a low viscosity fluid. These assumptions are expressed through the Rossby, $\mathrm{Ro}=U/\Omega R$ (U being the characteristic velocity of the fluid, as viewed in a reference frame rotating at Ω), and Ekman, $E=\mathrm{Re}_R^{-1}=\eta/\rho_f\Omega R^2$, numbers, respectively. According to the theory, when lowering the rotation frequency toward the critical frequency marking the onset of segregation (Ω_H in Fig. 1), the suspended particles in the initially axially independent distribution [Fig. 1(b)], periodically penetrate the rigidly rotating core of fluid. As a result inertial modes are continuously excited in the bounded cylinder, corresponding to the fre-

quency of the disturbance (in general, close to Ω) and to the particle trajectory features.

In some instances, such as for 3 mm polystyrene balls suspended in water, the particles' trajectory is almost circular, adjoining the cylinder wall [12]. In this case the trajectory strongly correlates the flow pattern in the perpendicular plane to the axis of rotation of a particular inertial mode—the $(1,1,n)$ mode[6] [11]. The rotating frame pressure and velocity fields associated with this mode are

$$p^{(1,1,n)} = P_0 J_1(\gamma r_R^*)\cos(\phi_R^* + t^*)\cos(kz_R^*),$$

$$u_r^{(1,1,n)} = \mathrm{Ro}\left[2\frac{J_1(\gamma r_R^*)}{\gamma r_R^*} + J_1'(\gamma r_R^*)\right]\sin(\phi_R^* + t^*)\cos(kz_R^*),$$

$$u_\phi^{(1,1,n)} = \mathrm{Ro}\left[2J_1'(\gamma r_R^*) + \frac{J_1(\gamma r_R^*)}{\gamma r_R^*}\right]\cos(\phi_R^* + t^*)\cos(kz_R^*),$$

$$u_z^{(1,1,n)} = \sqrt{3}\,\mathrm{Ro}\,J_1(\gamma r_R^*)\sin(\phi_R^* + t^*)\sin(kz_R^*), \tag{4}$$

here $\gamma = \sqrt{3}k$ and the amplitude of the scaled pressure perturbation is related to Ro through $P_0 = \frac{\gamma}{k^2}\,\mathrm{Ro}$. For this particular mode $\gamma = 2.74$ and thus $P_0 \cong 1.095\,\mathrm{Ro}$. The flow field corresponding to the above mode is *stationary* when viewed from the laboratory frame of reference. The velocity and pressure fields $(\hat{p}^*, \mathbf{u}^*)$ resulting from superimposing this mode on the rigidly rotating flow are

$$\hat{p}^* = \tilde{p}^* + \frac{\mathbf{g}\cdot\mathbf{r}^*}{\Omega^2 R} = \frac{r^{*2}}{2} + P_0 J_1(\gamma r^*)\cos(\phi^*)\cos(kz^*) - \frac{g}{\Omega^2 R} r^* \sin(\phi^*),$$

$$u_r^* = \mathrm{Ro}\left[2\frac{J_1(\gamma r^*)}{\gamma r^*} + J_1'(\gamma r^*)\right]\sin(\phi^*)\cos(kz^*),$$

$$u_\phi^* = r^* + \mathrm{Ro}\left[2J_1'(\gamma r^*) + \frac{J_1(\gamma r^*)}{\gamma r^*}\right]\cos(\phi^*)\cos(kz^*),$$

$$u_z^* = \sqrt{3}\,\mathrm{Ro}\,J_1(\gamma r^*)\sin(\phi^*)\sin(kz^*). \tag{5}$$

There is in general freedom in choosing the reference "horizon" for the azimuthal angle ϕ^*. Nevertheless, the gravity-induced trajectory of the suspended particles, which causes the excitation of the inertial modes, breaks this symmetry. Thus, in most experimentally studied cases the relevant horizon is the natural one (perpendicular to gravity) [9,12]. The projection of the velocity field in the vertical plane through the axis of rotation, onto the same plane, is depicted in Fig. 3(a). The perturbation pressure field (pertaining to the inertial mode) in the horizontal plane through the axis of rotation is shown in Fig. 3(b).

We now investigate qualitatively the character of the axial forces which correspond to the inertial mode. These are the

[6]The three indices represent the discrete integers which specify a particular inertial mode (in cylindrical coordinate representation).

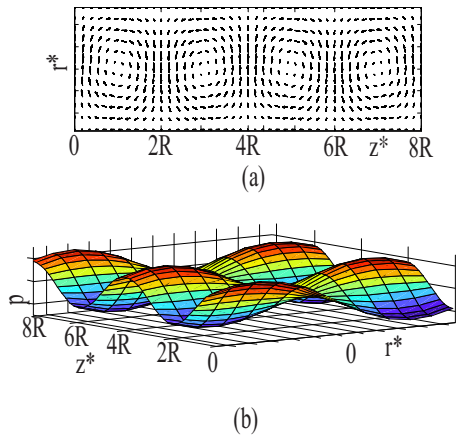

FIG. 3. (Color online) (a) Projection of the velocity field in the vertical plane through the axis of rotation, onto that plane. (b) Perturbation pressure in the horizontal plane through the axis of rotation.

axial component of the viscous drag, resulting from the axial velocity component of the mode excitation, and the force due to pressure gradients in the axial direction.

The axial component of the viscous drag will reflect the symmetry of the axial velocity component (u_z^*). The azimuthal dependence of the axial velocity component is antisymmetric with respect to the horizontal plane through the axis [Fig. 4(a)]. This implies that for almost circular off-centered trajectories, which are symmetric with respect to this plane, the drag corresponding to the axial flow would not be effective in causing particles to segregate into nodal planes; the net impulse in the upper half is exactly canceled by the net impulse imparted to the particle in the lower half. In general, though (for relatively small Π_5), the trajectories are somewhat inclined towards the lower half for negatively buoyant particles (upper half for positively buoyant). For these cases the effect of the drag is to carry the particles to

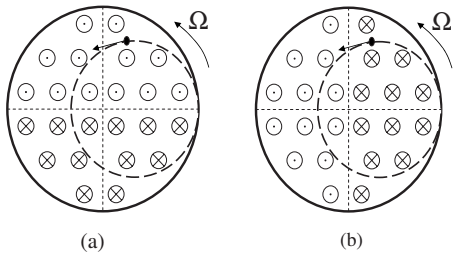

FIG. 4. Scheme of a circular trajectory of a suspended particle in a flow which consists of a superposition of solid body rotation and the flow generated by the $(1,1,n)$ inertial mode. (a) The axial component of the velocity field is indicated. The corresponding drag is in the same direction. The net impulse per revolution in this case is zero. (b) Same as (a), but for the axial component of the pressure gradient.

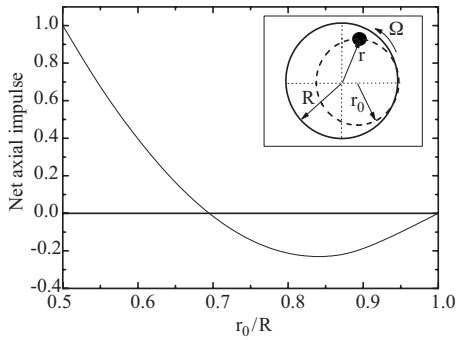

FIG. 5. Normalized net axial impulse acting on the suspended particle as a function of trajectory radius. The particle is assumed to undergo a circular uniform motion. Positive values correspond to stable bands for positively buoyant particles and vice versa.

nodes in which the flow pattern poorly correlates[7] their trajectory. This suggests that the viscous drag causes the bands to be unstable both for negatively and for positively buoyant particles. However, the fact that the trajectories adjoin the cylindrical surface has to be taken into consideration, since there the axial drag on the particle is different. This last fact might have considerable consequences for trajectories for which the adjoining segment is large. The scaled force due to the pressure gradient in the axial direction is

$$F_z^* = \Pi_2\left(-\frac{\partial p}{\partial z^*}\right) = 1.095\Pi_2 \,\mathrm{Ro}\, kJ_1(\gamma r^*)\cos(\phi^*)\sin(kz^*).$$

The expression is symmetric with respect to the horizontal plane through the axis of rotation and antisymmetric with respect to the vertical plane [Fig. 4(b)]. This implies that the pressure field is dominant in causing axial migration for the typical trajectory depicted in Fig. 4.

The net impulse on a particle having a circular trajectory tangential to the tube wall at one point has been calculated by integrating (2) numerically with respect to time. The particle is assumed to maintain a uniform velocity, in agreement with the empirical study of the motion of a single particle in a rigidly rotating tube [12]. Figure 5 shows the dependence of the net axial impulse (per revolution) on the particle as a function of the trajectory radius, r_0.

For trajectory radii r_0 larger than approximately $0.7R$ the net impulse due to pressure gradient in the axial direction acts to accumulate negatively buoyant particles in *alternate* nodal planes where the flow field correlates their trajectory, while for positively buoyant the effect is destabilizing. For radii smaller than $0.7R$, the situation is opposite. We emphasize that the above result is independent of the particle diameter or of its axial position. The fact that at the walls one can have either of the two flow patterns (see Fig. 12 in [12]), together with the fact that the axial forces accumulate particles into interleaving nodal planes, leads to two *degenerate* states for each resonant tube length.

[7] A quantitative measure of the correlation between the gravity-induced trajectory of the particle and the flow pattern of the inertial mode in the $r^*-\phi^*$ plane is given by the line integral over a closed trajectory: $\frac{1}{l}\oint \frac{\mathbf{r}^*\cdot\mathbf{u}^*}{\mathbf{u}^{*2}}\mathbf{dl}$, where l is the trajectory length.

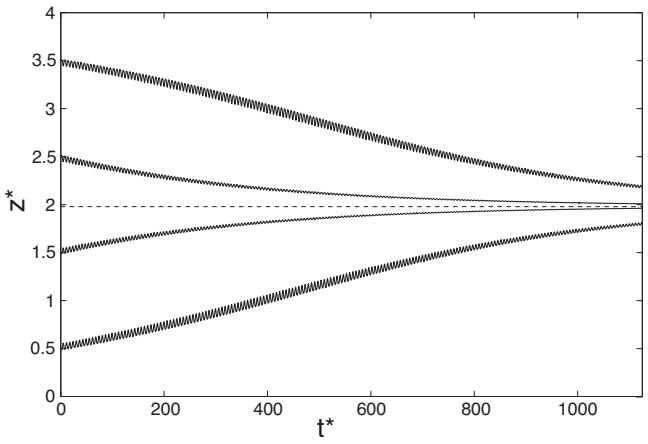

FIG. 6. Numerical simulation of the migration tendencies of a 1.59 mm Nylon ball placed in a flow field which consists of a superposition of solid body rotation and the $(1,1,n)$ inertial mode. Different initial positions result in migration to the same nodal plane ($z^* \cong 2$ in this instance) where the gravity-induced trajectory correlates the theoretical flow pattern. The Rossby number in this case is Ro=0.05.

B. Stability analysis

In Sec. III we have confirmed the validity of the approximate governing equation of motion for a single particle placed in an otherwise unperturbed rigidly rotating fluid through numerically integrating Eq. (2). Using the same numerical code we can now investigate the different possible segregation scenarios determined by the interplay between the two axial forces which correspond to the $(1,1,n)$ inertial mode excitation. To this end we assume that the bands have already formed and the $(1,1,n)$ inertial mode excited, and focus our attention on a single test particle experiencing the theoretical field. This would correspond to following one of the suspended particles, which has found itself distant from the center of its original band. We investigate whether the particle will tend back toward the nodal plane, where the band resides and where its trajectory correlates the flow field in the $r-\phi$ plane, or migrate toward the neighboring nodal plane where its trajectory poorly correlate the flow filled.

Figure 6 presents the axial position as a function of time for a 1.59 mm Nylon balls suspended in a 55.8 mm water-filled rotating horizontal cylinder. The rotation rate is 4.9 rad/s. Four different cases, corresponding to four different initial axial positions are shown. The oscillations seen in the figure reveal the azimuthally dependent resultant axial force acting on the particles.

The figure clearly shows the tendency of the particles to migrate towards *interleaving* nodal planes (represented by a broken line) where the flow pattern correlates the gravity-induced trajectory of the particles, in agreement with the theory. The migration tendency is enhanced for higher amplitudes of the perturbing inertial mode (i.e., for higher Ro).

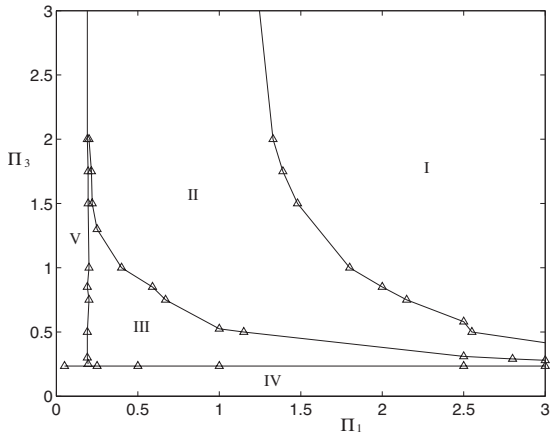

FIG. 7. Phase diagram in the Π_1-Π_3 plane depicting the different possible trajectory scenarios of a single particle in a flow field which consists of a rigid rotation and the flow due to the $(1,1,n)$ inertial mode. These are the pinned to wall (I), the stationary and axially stable (II), the stationary and axially unstable (III), the stuck to bottom (IV), and the spiral motion toward a fixed point (V).

In Sec. II, we presented the six independent dimensionless parameters which determine whether for a given system segregation and formation of bands will be observed. Once these parameters are determined a point in the corresponding parameter space is defined. This point corresponds to one of the four possible situations depicted in Fig. 1. Of particular interest are the points which correspond to a stable band pattern [Fig. 1(c)]. In the first part of the present section we have numerically integrated Eq. (2) for a single particle suspended in a flow which consists of a superposition of solid body rotation and the field corresponding to the dominant inertial mode [i.e., the $(1,1,n)$ mode]. In this way we could investigate the migration tendencies in the axial direction, which provided further confirmation of the theoretical framework. We now use this strategy in an attempt to explore the different regimes in parameter space and in particular the boundaries of the stability region.

As the problem consists of several parameters, we will focus on the stability diagram in the Π_1-Π_3 plane. In this plane the interfaces of the different regimes are most clearly revealed. In Fig. 7 we present the results of the investigation of the different regimes corresponding to the projection of the space onto the Π_1-Π_3 plane, for the specific case: $\Pi_5=100$, $\Pi_2=0.2$, and $\mathrm{Ro}=0.05$. The aspect ratio, $R/d=(\Pi_3/18\Pi_2)\Pi_5$, was in this case set to 20. This last specification enters the simulation explicitly as a closest approach limit in the encounter with the wall. The wall-drag numerical parameter (β_1), depicting the extent to which the drag in the close vicinity to the wall differs from the drag far from the wall, was set to unity. The numerical parameter representing the depth of the boundary layer (β_2) was set to unity, too. This relatively high value was chosen in order to emphasize the destabilizing effect of the segment of the trajectory adjacent to the cylinder wall (through the action of the axial component of the viscous drag).

Examining the diagram we see four regions representing different trajectory scenarios which correspond to the four time-independent states depicted in the graphical illustrations of Fig. 1. These are the pinned to wall (I), the stationary and axially stable (II), the stationary and axially unstable (III), and the stuck to bottom (IV) regions. A fifth region (V), representing transient spiral motion towards a fixed point, could stand for any of the three states corresponding to the three adjoining sections, depending on the value of Π_3.

The interface between the region corresponding to sedimentation and the regions corresponding to stationary but unstable bands and thin coating is an almost horizontal line $(\Pi_3 \cong 0.25)$. In a similar way, the interface between the region representing spiral motion onto a fixed point (V), and the two adjoining zones [i.e., those corresponding to stationary and axially stable (II) and stationary and axially unstable (III)] is an almost vertical straight line $(\Pi_1 \cong 0.2)$. The interface between the region corresponding to thin coating and the regions representing stationary trajectories (corresponding to stable and unstable bands) was determined by the somewhat arbitrary condition that the particles will not only detach but achieve a distance of at least one diameter (d) from the wall. This is in accordance with the assertion that the particles need to penetrate the fluid in order to excite resonant modes.

V. DISCUSSION

A dimensionless analysis of the phenomenon of segregation and formation of axial bands in a suspension-filled rotating horizontal cylinder was presented. The six independent dimensionless parameters associated with this intriguing phenomenon were identified and their significance, as well as the significance of other dimensionless parameters which can be obtained by a combination of this set (e.g., the Stokes number), explained. An approximate dimensionless equation of motion for a single particle suspended in a rotating fluid-filled tube, based on an empirical law for the viscous drag, was given. The equation was integrated numerically and the corresponding trajectory shown to be in good agreement with experimental results for relatively high Reynolds numbers $[\Pi_5=O(100)]$.

The detailed mechanism of segregation and formation of bands was presented for small Ekman and Rossby numbers. The axial forces related to the dominant inertial mode excitation [i.e., the $(1,1,n)$ mode] within the bounding fluid were examined with regard to their influence on the formation of a stable band pattern. The axial pressure gradient associated with the inertial mode was shown to be the main driving force causing migration into interleaving nodal planes where the gravity-induced motion of the suspended particles correlates the flow field. The trajectories of suspended test particles in the theoretical field which consisted of the mode excitation superimposed on a solid body rotation were investigated numerically and have further confirmed the theoretical approach. The stability of the band patterns was examined by numerically integrating the approximated dimensionless equation of motion for a test particle. This also allowed for the construction of the dimensionless phase space corresponding to the banding phenomenon.

The Rossby number (Ro), defined when dealing with the Navier-Stokes equation (rotating frame), is not an independent dimensionless number but depends on the six dimensionless numbers presented in Sec. II. In fact, for a single mode excitation, for which Ro is the scaled amplitude of the perturbation velocity, we have a closed form assuming a time periodic driving force acts on the fluid [19],

$$\mathrm{Ro} = \frac{\int \mathbf{F}(\mathbf{r}) \cdot \mathbf{U}(\mathbf{r}) dV}{[i(\alpha - 1) - E^{1/2}s] \int \mathbf{U}(\mathbf{r})^{\dagger} \cdot \mathbf{U}(\mathbf{r}) dV}. \quad (6)$$

Here $\mathbf{F}$ is the force acting on the fluid, having a harmonic time dependence of dimensionless frequency α, $\mathbf{U}(\mathbf{r})$ is the spatial component of the inertial mode velocity field, and s can, in principle, be calculated knowing the flow field resulting from our particular mode [see Eq. (2.9.12) of [19]]. The driving force would in our case represent the persistent periodic disturbance caused by the suspended particles. An approximate expression for $\mathbf{F}$ could be that of a point force acting at the instantaneous positions of the suspended particles, in which case the correlation between the particles' instantaneous velocities and the theoretical velocity field at the same points would be the prime ingredient in the numerator of Eq. (6). It would then be possible to numerically simulate the evolution of the suspended particles' distribution from an initially homogeneous state,[8] in a field which consists of a superposition of the inertial mode perturbation[9] and a rigid rotation. The perturbation amplitude would be fedback at each time step from the collective correlation of the particles' instantaneous velocities and the corresponding flow field at the previous time step.

It is worth noting the insight given by Eq. (6) into the role of the dimensionless numbers Π_4 and Π_6. The numerator will be proportional to the volume fraction (Π_4) through the force exerted by the particles and therefore so will the Rossby number. For very low values of Π_4, the suspended particles can no longer be viewed as a continuum and the prospects of exciting inertial modes diminish. This is the case, for instance, for 3 mm polystyrene balls suspended at very low volume fractions in a water-filled horizontal cylinder. We have mentioned earlier that one observes experimentally a strong correlation between discrete values of the aspect ratio $\Pi_6 = L/R$ (i.e., $L/R \cong 2n$), and the intriguing phenomenon of oscillating band patterns. In light of Eq. (6), this might be related to the fact that at these values one has an optimal correlation between $\mathbf{F}(\mathbf{r})$ and the $(1,1,n)$ inertial mode field, $\mathbf{U}(\mathbf{r})$ (the wavelength of the mode being equal to $3.97R$), which is manifested by a peak in the corresponding Rossby number.

The stability analysis presented in Sec. IV B. is based on the underlying assumption that a sufficient number of suspended particles [that is, $\Pi_4 \sim O(10^{-2})$] excite the $(1,1,n)$ inertial mode due to their gravity-induced trajectory which correlates the flow field in interleaving nodes of the excitation. This assumption might not be valid for stationary trajectories which have an effective frequency appreciably different than Ω, or which poorly correlate the flow field of the dominant mode excitation in the $r^* - \phi^*$ plane. Thus, the area in the vicinity of the intersection point between the $\Pi_1 \cong 0.2$ and $\Pi_3 \cong 0.25$ lines, which lies in region III ("stationary and axially unstable") of Fig. 7, and for which the particle's closed trajectory only slightly penetrates the core, might not adequately represent the corresponding state of the large system.

APPENDIX

In order to derive the six dimensionless numbers presented in Sec. II, we start with choosing three dimensional numbers having independent units, out of the nine which define the system. These are R, Ω, and ρ_f. This choice is not unique, nor is the set of dimensionless numbers it yields. Next, we scale the six dimensional parameters left to obtain the following independent set of dimensionless parameters:

$$\Psi_1 = \frac{\rho_p}{\rho_f}, \quad \Psi_2 = \frac{\Delta\rho g}{\rho_f \Omega^2 R}, \quad \Psi_3 = \frac{\eta}{\rho_f \Omega R^2}, \quad (A1)$$

$$\Psi_4 = \frac{V_p}{R^3}, \quad \Psi_5 = \frac{d}{R}, \quad \Psi_6 = \frac{L}{R}.$$

The more physically insightful independent dimensionless set used in our work is derived from Eq. (A1) by the following transformation:

$$\Pi_1 = \Psi_1 \Psi_2^{-1}, \quad \Pi_2 = \Psi_2^{-1}, \quad \Pi_3 = 18 \Psi_2^{-1} \Psi_3 \Psi_5^{-2},$$

$$\Pi_4 = \pi^{-1} \Psi_4 \Psi_6^{-1}, \quad \Pi_5 = \Psi_3^{-1} \Psi_5, \quad \Pi_6 = \Psi_6. \quad (A2)$$

[8] Equation (6) gives the perturbation amplitude after a transient (spin-up) time has elapsed from the application of the driving force. It therefore would faithfully convey the actual amplitude providing the evolution toward the band pattern is slow in comparison to the spin-up time, $E^{-1/2}\Omega^{-1}$.

[9] Or, of a number of potentially excitable modes [in which case Eq. (6) would give the amplitude of a particular mode].

[1] H. G. Ristow, *Pattern Formation in Granular Material* (Springer, Berlin, 2005).
[2] M. Tirumkudulu, A. Tripathi, and A. Acrivos, Phys. Fluids **11**, 507 (1999); **11**, 1962 (1999), erratum.
[3] M. Tirumkudulu, A. Mileo, and A. Acrivos, Phys. Fluids **12**, 1615 (2000).
[4] O. A. M. Boote and P. J. Thomas, Phys. Fluids **11**, 2020 (1999).
[5] P. J. Thomas, Phys. Fluids **13**, 2720 (2001).
[6] S. G. Lipson, J. Phys.: Condens. Matter **13**, 5001 (2001).

[7] S. G. Lipson and G. Seiden, Physica A **314**, 272 (2002).
[8] A. P. J. Breu, C. A. Kruelle, and I. Rehberg, Europhys. Lett. **62**, 491 (2003).
[9] W. R. Matson, B. J. Ackerson, and P. Tong, Phys. Rev. E **67**, 050301(R) (2003).
[10] J. Lee and A. J. C. Ladd, Phys. Rev. Lett. **89**, 104301 (2002).
[11] G. Seiden, S. G. Lipson, and J. Franklin, Phys. Rev. E **69**, 015301(R) (2004).
[12] G. Seiden, M. Ungarish, and S. G. Lipson, Phys. Rev. E **72**, 021407 (2005).
[13] E. Buckingham, Phys. Rev. **4**, 345 (1914).
[14] G. O. Roberts, D. M. Kornfeld, and W. W. Fowlis, J. Fluid Mech. **229**, 555 (1991).
[15] R. Clift, J. R. Grace, and M. E. Weber, *Bubbles drops and particles* (Academic, New York, 1978).
[16] C. J. Lawrence and R. Mei, J. Fluid Mech. **283**, 307 (1995).
[17] G. G. Joseph, R. Zenit, M. L. Hunt, and A. M. Rosenwinkel, J. Fluid Mech. **433**, 329 (2001).
[18] G. G. Joseph and M. L. Hunt, J. Fluid Mech. **510**, 71 (2004).
[19] H. P. Greenspan, *The Theory of Rotating Fluids* (Springer, Berlin, 1993).